Microsc. Microanal. Microstruct. **4** (1993) 221–237 APRIL/JUNE **1993**, PAGE 221

Classification
Physics Abstracts
61.70J — 61.70N

Interaction between dislocations and $\Sigma = 51$ and $\Sigma = 19$ tilt grain boundaries in germanium: Study by *in-situ*, TEM and HREM

H.M. Michaud([1])(*), X. Baillin([1]), J. Pelissier([1]), J.L. Putaux([2]) and J. Thibault([2])

([1]) CEA/CEREM/Département d'Etudes des Matériaux, CENG, 85X-38041 Grenoble, France
([2]) Département de Recherche Fondamentale sur la Matière Condensée, SP2M/S, CENG, 85X-38041 Grenoble, France

(Received February 5, 1993; accepted May 22, 1993)

Résumé. — Les bicristaux de flexion autour de [011] $\Sigma = 51$ et $\Sigma = 19$ ont été déformés *in-situ* au microscope 1 Mev. Les différentes configurations résultant de l'interaction des dislocations induites par la déformation et le joint de grains ont été caractérisées par MET. On a aussi étudié par MEHR un événement observé *in-situ* correspondant à l'entrée d'une dislocation dans le joint. De ces observations il résulte que i) les configurations correspondant à des transmissions diffèrent fortement en fonction des conditions de déformations, ii) dans ces joints les transmissions observées ne correspondent pas à des transmissions directes de dislocations. Les dislocations sont incorporées au joint où elles se décomposent ; l'émission de dislocations s'effectuant après l'accumulation de plusieurs dislocations dans le joint.

Abstract. — The deformation of two different tilt bicrystals $\Sigma = 51$ et $\Sigma = 19$ has been studied by 1 Mev *in-situ* electron microscope. The configurations resulting from the interaction between the dislocations induced by the deformation and the GBs have been characterised by TEM. HREM has been used to study a single impact detected previously during the in situ experiment. From these observations it has to be pointed out that i) the configurations resulting from the transmission or the emission of dislocations are different depending on the deformation conditions, ii) the incoming dislocations enter the GB where they decomposed into residual GB dislocations, the emission of dislocations from the GBs resulting from the accumulation of dislocations into the GB.

1. Introduction.

Numerous results has been already obtained on the deformation of the so-called favoured GB : $\Sigma = 9$ tilt GB in germanium or silicon. The behaviour of this $\Sigma = 9$ tilt GB has been extensively studied by *in-situ* 1 MEV electron microscopy and X-rays topography [1-3]. Its structural evolution has been studied by HREM as well [4-6]. We concluded that i) this $\Sigma = 9$ GB was a strong obstacle with respect to the slip transmission ii) the deformation induced dislocations enter the GB plane

(*) *present adress:* ALCATEL/Fibres optiques, 35 r. J. Jaurès, BP115, 95874 Bezons-F

where they decomposed into elemental GB dislocations (GBDs) whose Burgers vector belongs to the $\Sigma = 9$ DSC lattice but is not necessary the smallest vector iii) the structural evolution of the deformed GB and its content in GB dislocations was in agreement with the Sutton and Vitek [7] description in terms of structural units.

As $\Sigma = 51$ and $\Sigma = 19$ are not special GBs, the aim of the present paper is to achieve a more general description of behaviour of the GBs submitted to a deformation.

2. Experimental.

2.1 MACROSAMPLES. — Germanium bicrystals has been grown by the Czochralsky method. The geometrical characteristics of the two GBs are given in table I. Macrosamples $\left(14.5 \times 3.5 \times 3.5\ mm^3\right)$ has been predeformed in compression under 20 MPa at a 0.15 % strain.

Table I. — *Geometrical (grain I as reference) and energetical characteristics of the two original GBs as compared to those of the favoured $\Sigma = 9$ GB.*

GBs	θ (°)	GB plane	GB period	GB energy ($J m^{-2}$)
51	16.10	$(\bar{1}\,5\,\bar{5})$	a/2 $[10\,1\,\bar{1}]$	0.320
19	26.52	$(\bar{1}\,3\,\bar{3})$	a/2 $[6\,1\,\bar{1}]$	0.256
9	38.94	$(\bar{1}\,2\,\bar{2})$	a/2 $[4\,1\,\bar{1}]$	0.222

2.2 MICROSAMPLES. — Micro samples $\left(6.5 \times 2 \times 0.7\ mm^3\right)$ for *in-situ* experiments has been extracted from macrosamples in such a way that the GB is either parallel or perpendicular to the tensile axis in the microscope.

They are thinned with a 7 μm SiC powder in water until a 80 μm thickness is reached. They are subsequently polished with 6 μm and 1 μm diamond powders till 70 μm.

In order to locate the observation hole before ion milling, the GB is revealed chemically. The hole must be located such as the stress is maximum close to the GB [8]. The two geometrical samples configurations are showed in figure 1. In the case of the longitudinal GB (Fig. 1a), the GB is inclined with respect to the sample surface.

In order to fix the sample in the tensile stage of the microscope, two holes 0.45 mm in diameter are made 5 mm apart.

2.3 IN-SITU EXPERIMENTS. — The 1 Mev electron microscope is operating at 400 kV in order to avoid radiation damages in the germanium. The vacuum is held at 5×10^{-7} torr during tensile tests. The tensile heating double tilt goniometer stage has been described elsewhere [9] The possibilities and the actual conditions used in these experiments are described in table II.

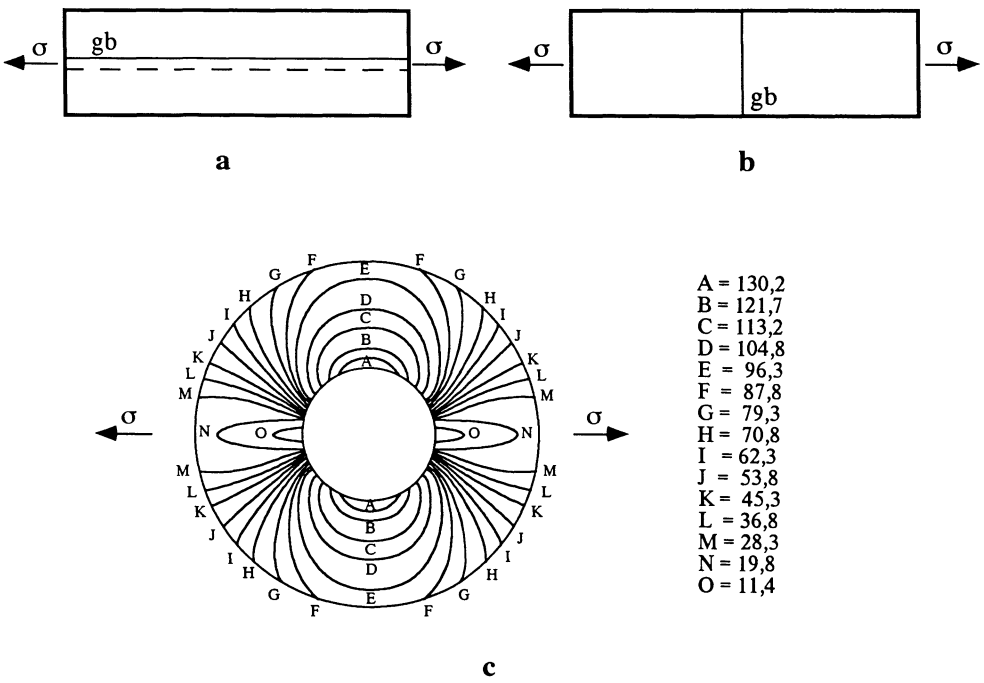

Fig. 1. — Microsamples for the *in-situ* experiments in the case of the longitudinal GB (a) and the transverse GB (b). c) Iso-stress map (MPa) around the hole [8] shows that the stress is maximum on both sides of the hole. Consequently, the longitudinal GB must be located as it is tangent to the hole (a).

Table II. — *Experimental features of the in-situ experiments.*

	Possibilities	Experimental conditions (Ge)
voltage	1 MV	400 kV
furnace	1000 K	0.7Tm ≈ 780K
load	100 ± 0.02g	σ ≈ 50MPa /8/
extension	1.3mm	20μm
double tilt	xx' ±35° yy' ±10°	2-beams on the two grains simultaneously

2.4 MET AND HREM OBSERVATIONS. — 3 mm diameter discs were cut in the *in-situ* deformed micro samples. They have been characterized by MET using a JEOL 200CX equiped with a double tilt goniometer (±60°, ±30°). The HREM observations were carried out on a JEOL 200CX (Cs = 1 mm) equipped with a top entry goniometer. The HREM image simulations have been performed using the EMS package by Stadelmann [10].

3. $\Sigma = 51$ and $\Sigma = 19$ structure determination.

The structure of the two GBs was determined before any deformation. Thanks to the previous results obtained on the $\Sigma = 9$ GB, the structural models of the two GBs were assumed to fulfilled the mixing rule of SUs given by Sutton and Vitek [7]. Thus, as the misorientation angles of the two GBs are between those of the two favoured GBs : $\Sigma = 1$ ($\theta = 0°$) and $\Sigma = 9$ ($\theta = 38.94°$) made with only one SU : C and L respectively, then the periods of $\Sigma = 51$ and $\Sigma = 19$ are made with a mixture of the L and C SUs. The two structures have been relaxed by atomistic calculations [11, 12] the two GBs given in table I are larger as compared to $\Sigma = 9$ one.

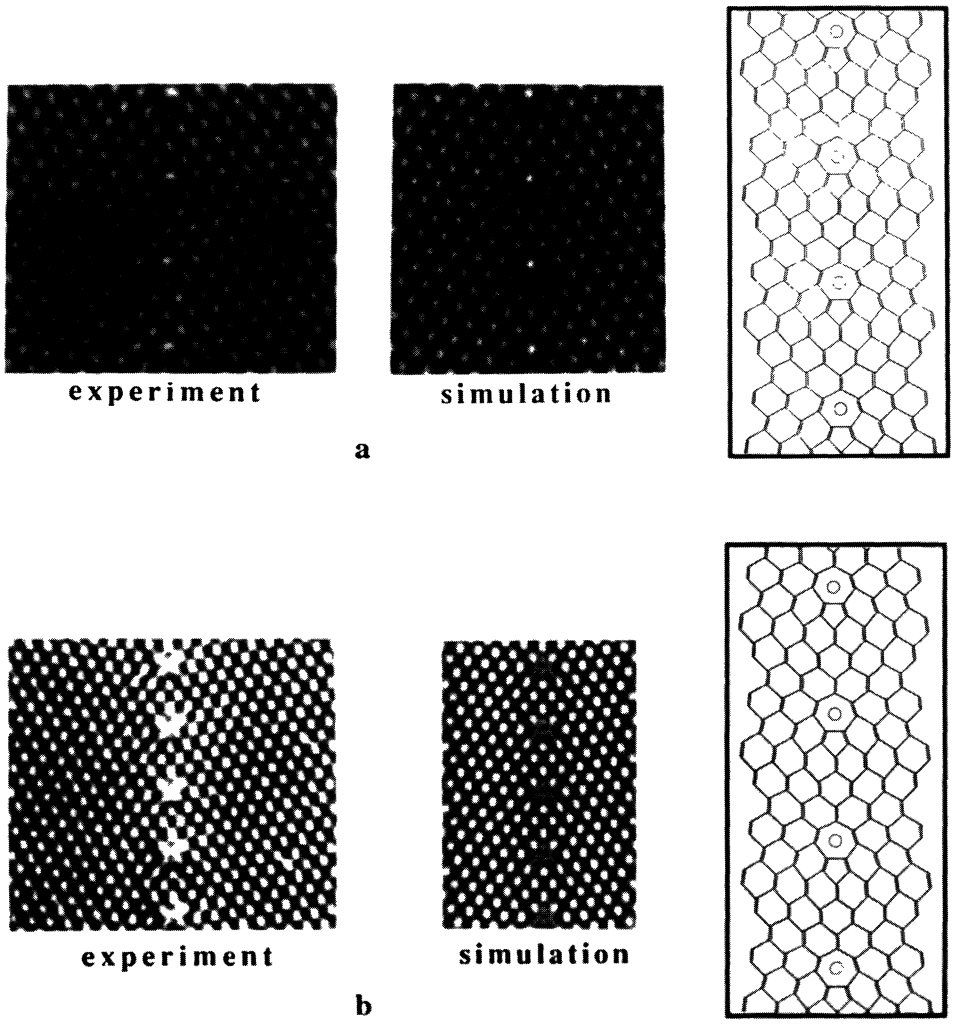

Fig. 2. — $(\bar{1}55)$ [011] $\Sigma = 51$ GB : comparison between the experimental through focus series and the computed ones (200 kV, $Cs = 1.05$ mm, $\alpha = 1$ mrd, $\delta z = 7$ nm, objectif aperture $= 10\ \text{nm}^{-1}$, thickness: 5 nm).
a) black atoms: $\Delta z = 40$ nm, b) white atoms: $\Delta z = 0$ nm, . The structure is shown in the frame.

3.1 $(\bar{1}55)$ [011] $\Sigma = 51$. — In order to determine the structure without ambiguity, two images at different focus were performed in the microscope. The resulting images were compared with the simulated images computed with the relaxed atomic model corresponding to the SU mixing rule : the theoretical GB period is the following:

$$\{CCCLCCCL\}$$

Figure 2 shows the comparison between the experimental and the computed images. The agreement is very good and one can be confident with the structure of the GB.

3.2 $(\bar{1}33)$ [011] $\Sigma = 19$. — In this case two images at two different focus were performed as well. The resulting images has been compared with the simulated images computed with the atomic model corresponding to the SU mixing rule which gives the following GB period:

$$\{CLCL\}.$$

Figure 3 shows the comparison between the experimental and the computed images.

4. In-situ deformation.

4.1 DEFORMATION CONDITIONS. — For the first time, Bacmann *et al.* [15] showed experimentally that the misorientation angle θ between the two grains varies as a bicrystal is strained symmetrically. Figure 4 shows the two deformation configurations as θ increases (4a) or decreases (4b). In fact, these conditions are imposed by the sign of the Burgers vector (BV) of the deformation induced dislocations. The deformation conditions are described in table III. The fact that the staking fault of the dissociated dislocation induced by the deformation is known to be intrinsic imposes the position of the two partials with respect to the GB. As θ increases, the dissociated dislocation comes towards the GB with the 90° partial as the head partial whereas the 90° is the trailing partial as θ decreases.

In the following we shall describe the experimental results for the different deformation conditions.

Table III. — Deformation conditions for the two bicrystals.

Σ	σ (90° head partial)	σ (30° head partial)
51	$[1\bar{5}5]_{I} = [\bar{1}\bar{5}5]_{II}$	$[\bar{5}23]_{I} = [\bar{5}32]_{II}$
19	$[1\bar{3}3]_{I} = [\bar{1}\bar{3}3]_{II}$	$[\bar{3}12]_{I} = [\bar{3}21]_{II}$

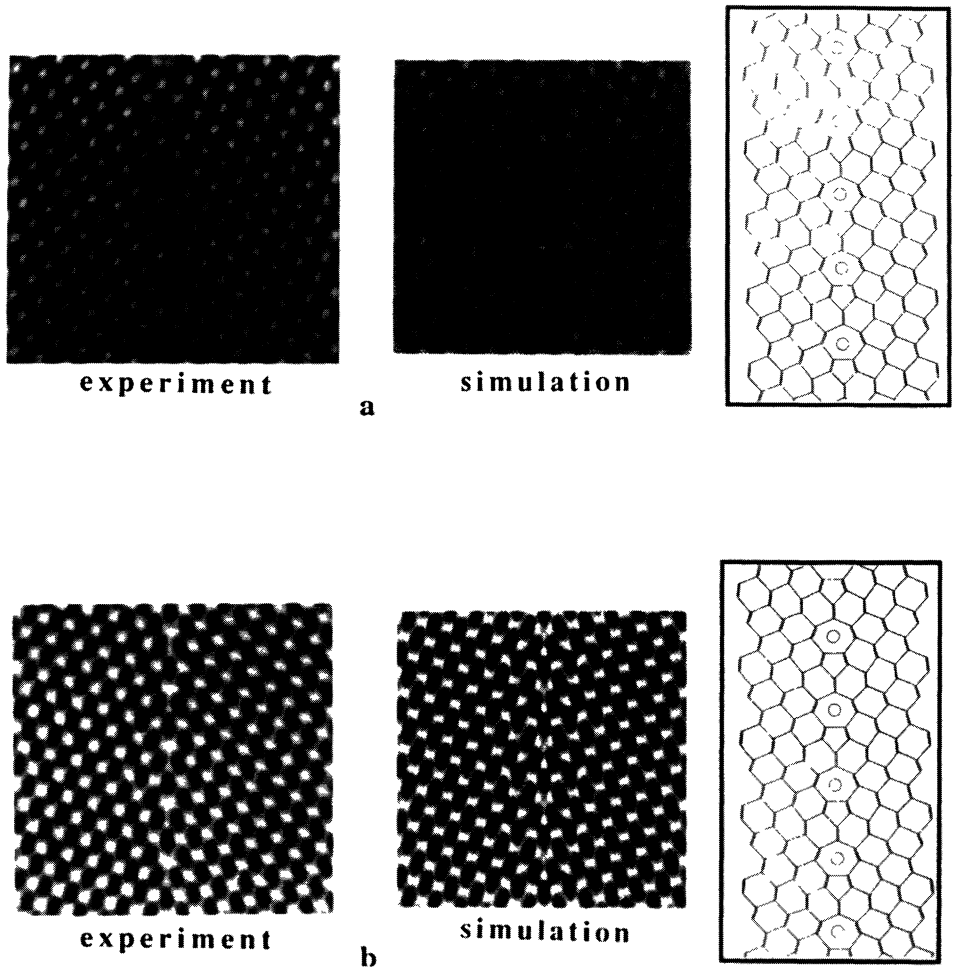

Fig. 3. — $(\bar{1}33)$ [011] $\Sigma = 19$ GB : comparison between the experimental through focus series and the computed ones (400 kV, $Cs = 1$ mm, $\alpha = 0.7$ mrd, $\delta z = 7$ nm, objectif aperture $= 11\ \mathrm{nm}^{-1}$, thickness: 5 nm). a) black atoms: $\Delta z = 40$ nm, b) white atoms: $\Delta z = -70$ nm, . The structure is shown in the frame.

4.2 $\Sigma = 51$ DEFORMATION: IN-SITU AND TEM CHARACTERISATION.

4.2.1 *90° partial as the head partial.* — In this case the sample normal is $[5\bar{4}\bar{5}]_{\mathrm{I}} = [5\bar{5}\bar{4}]_{\mathrm{II}}$, and the tensile stress in the microscope is applied along $[1\bar{5}5]_{\mathrm{I}} = [\bar{1}\bar{5}5]_{\mathrm{II}}$. In these conditions only one slip system is activated. Pile-ups of dislocations on $(11\bar{1})_{\mathrm{I}}$ coming towards the GB are formed. Figure 5 shows a series of micrographs from the *in-situ* sequence. The diffraction conditions are such that the dislocations must remain in contrast. After the accumulation of eleven dislocations in the GB, a dislocation is emitted in the adjacent grain on $(11\bar{1})_{\mathrm{II}}$. This dislocation remains linked to the GB by a stacking fault. A second dislocation is emitted which pushes the first emitted dislocation. The apparent width of the staking fault varies.

The BV of the in-coming dislocations has been characterised (Fig. 6) by TEM (extinction by $g = [220]_{\mathrm{I}}$). The total BV is $\pm 1/2\,[\bar{1}10]_{\mathrm{I}}$: the sign is determined by the Peach-Koehler force

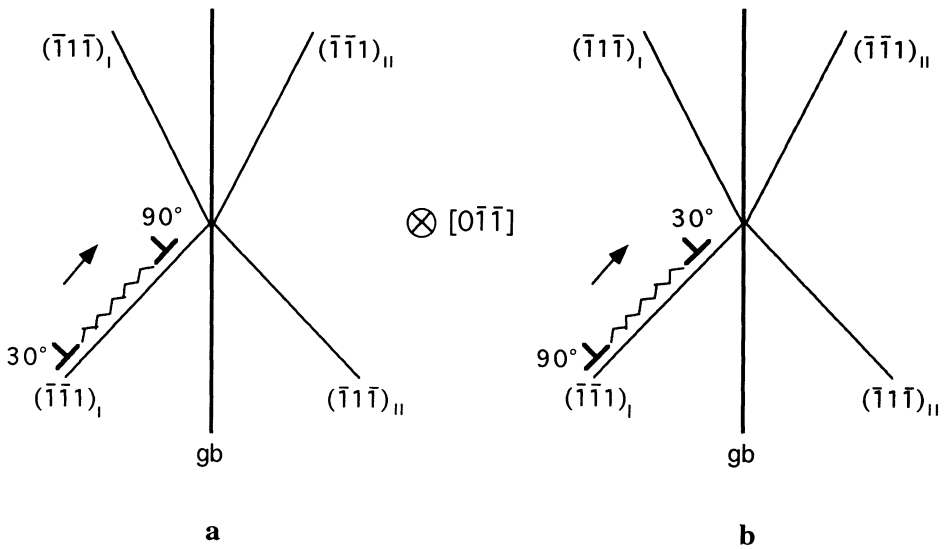

Fig. 4. — Deformation conditions under which θ increases (a) or decreases (b). As the dislocations are dissociated, the 90° partial is the head partial in (a) and the trailing partial in (b).

calculation. The head partial is $1/6\,[\bar{2}1\bar{1}]_I$ and the leading partial is $1/6\,[\bar{1}21]_I$. It has to be noticed that these BVs belongs to the $\Sigma = 51$ DSC lattice.

Three partial dislocations were emitted and their BV has been determined using the weak-beam technique. As the dislocations are in contrast with $[220]_{II}$, $[202]_{II}$ and $[\bar{1}3\bar{1}]_{II}$ and out of contrast with $[131]_{II}$ it follows that the BVs are identical: $1/6\,[\bar{2}1\bar{1}]_{II}$. This BV does not belong to the DSC lattice. the nature of the staking fault (SF) between the second and the third partial is extrinsic. Image simulations of the SF are also consistent with two intrinsic SFs on two close $(11\bar{1})_{II}$ planes. This last hypothesis is sustained by HREM observations [16].

4.2.2 *30° partial as the head partial.* — In this case the tensile stress in the microscope is applied along $[\bar{5}23]_I = [\bar{5}32]_{II}$. The sample normal is chosen to be $[47\,377\,\overline{173}]_I = [37\bar{3}]_{II}$: thus the GB plane is slightly inclined with respect to the sample surface (25°) and it is possible to put it perpendicularly to the electron beam in the microscope in order to be able to use the 022 common beam. In these conditions only one slip system on $(11\bar{1})_I$ and $(1\bar{1}1)_{II}$ planes (same as in §4.2.1) is activated. Pile-ups of dislocations on $(11\bar{1})_I$ coming towards the GB are formed. Figure 7 shows a series of micrographs from the *in-situ* sequence. Unlike in the case where the 90° is the head partial, perfect dislocations are successively emitted on the $(1\bar{1}1)_{II}$ plane from the GB at the impact point of the pile-up in grain I. Emission of perfect dislocations on the $(11\bar{1})_{II}$ also occurs. Double cross-slip from $(11\bar{1})_I$ to $(111)_I$ can be shown clearly on the sequence as well..

The TEM observations (Fig. 8) confirm that the BV of the incoming dislocations is $1/2\,[1\bar{1}0]_I$. They are dissociated into two partials. The 30° head partial is $1/6\,[1\bar{2}\bar{1}]_I$ and $1/6\,[2\bar{1}1]_I$ is the trailing partial. The emitted perfect dislocations can be viewed clearly. Furthermore, numerous grain boundary dislocations are emitted in the GB plane from the impact point of the in-coming pile-up.

4.3 $\Sigma = 19$ DEFORMATION: IN SITU AND TEM CHARACTERISATION. — For $\Sigma = 19$ the only case studied was the one where the leading partial is the 90° partial.

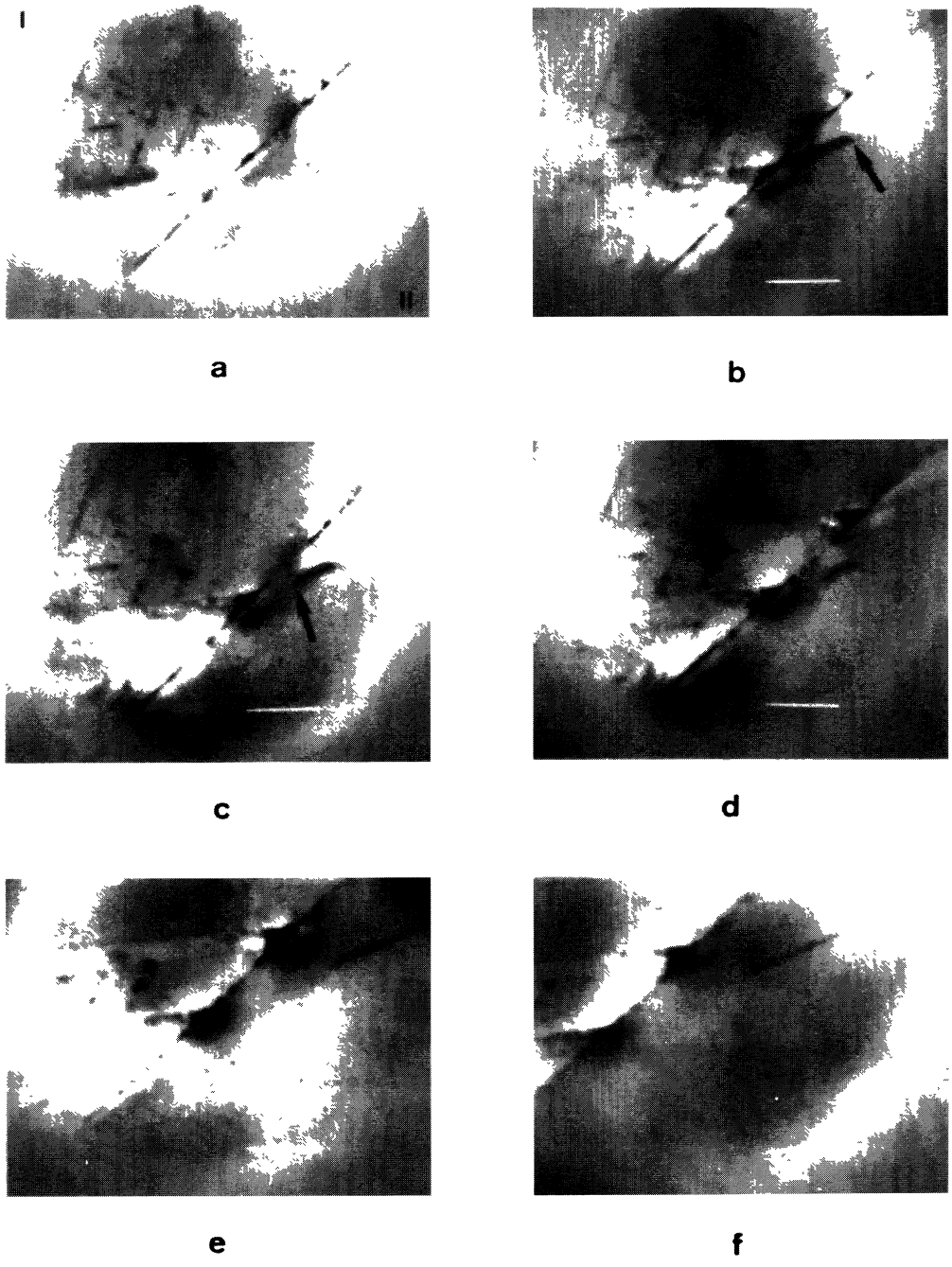

Fig. 5. — $\Sigma = 51$ in-situ deformation sequence in the conditions where the 90° partial is the head partial (θ increases). $g_{\mathrm{I}} =$ [202] and $g_{\mathrm{II}} =$ [220]. Marker = 1 μm.

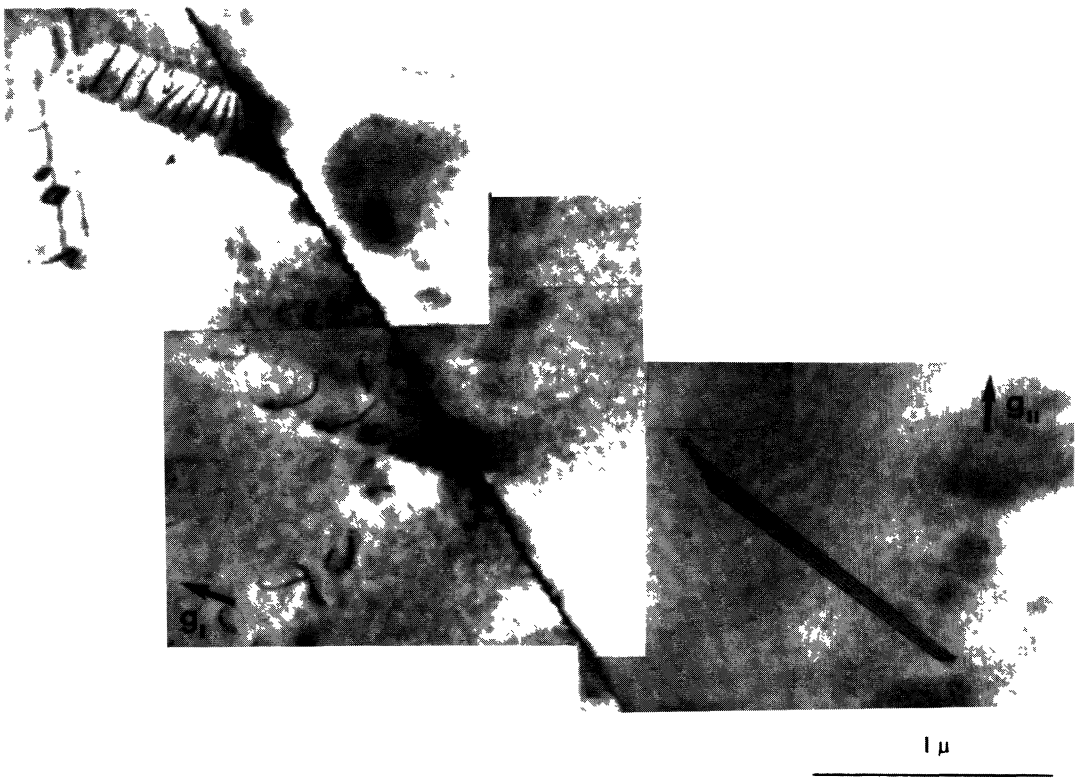

Fig. 6. — TEM observation of the configurations resulting from the interaction between $\Sigma = 51$ and the induced dislocations when the head partial is the 90° one. $g_I = [202]$, $g_{II} = [220]$.

In this case the sample normal is $[332]_I = [323]_{II}$, and the tensile stress in the microscope is applied along $[1\bar{3}3]_I = [\bar{1}\bar{3}3]_{II}$. The two diffraction vectors $[\bar{2}20]_I$ and $[\bar{2}02]_{II}$ in the sample plane make a 81° angle. Due to a parasitic reflexion, in these conditions the technique using the two beams conditions on the two grains simultaneously is difficult to be applied: this explains the bad quality of the images. Nevertheless in the deformation conditions, only one slip system is activated. Pile-ups of dislocations on $(11\bar{1})_I$ coming towards the GB are formed. Figure 9 shows a series of micrographs from the *in-situ* sequence.

After a pile up of twenty dislocations formation, two perfect dislocations were emitted in the adjacent grain on the $(11\bar{1})_{II}$ planes with a delay of one second between them. After one minute, (during which the pile up still growed) a perfect dislocation loop appeared on the $(111)_I$ plane.

Figure 10 (a,b) shows the TEM characterisation of the emitted dislocations and the loop.

5. $\Sigma = 51$: in situ deformation and HREM observation.

5.1 IN-SITU EXPERIMENTAL CONDITIONS. — The bicrystals were predeformed in compression perpendicularly to the GB at a 0.25% strain at 743 K. Microsamples containing a transverse GB (as shown in Fig. 1b) with a [011] normal (suitable for HREM observations) were extracted from the bicrystals. *In-situ* observations at 773 K were carried out in the following conditions: samples inclined of 33° with respect to the [011] axis and $g_I = [\bar{2}02]$ and $g_{II} = [\bar{2}20]$.

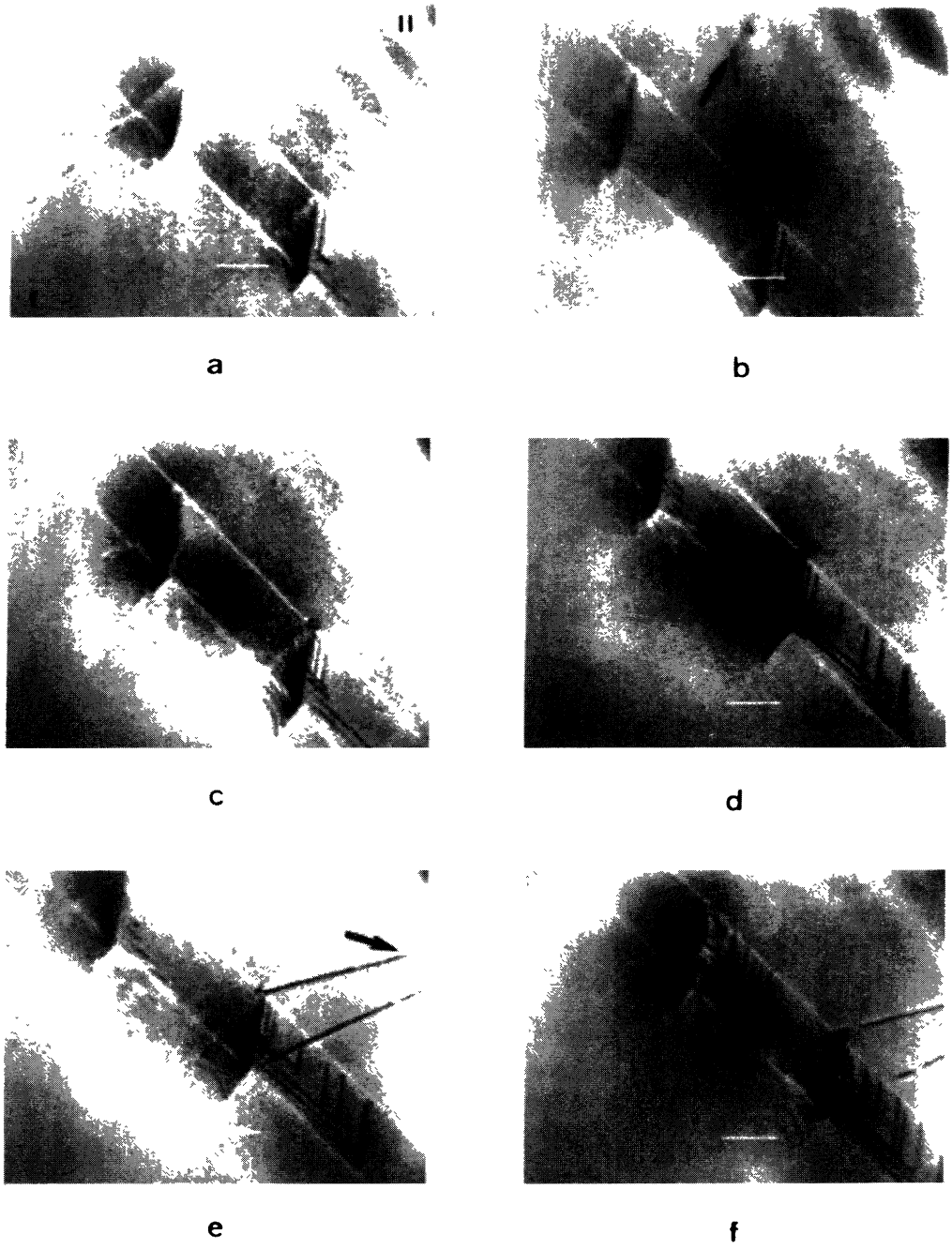

Fig. 7. — $\Sigma = 51$ *in-situ* deformation sequence in the conditions where the 30° partial is the head partial (θ decreases). Marker = 1 μm.

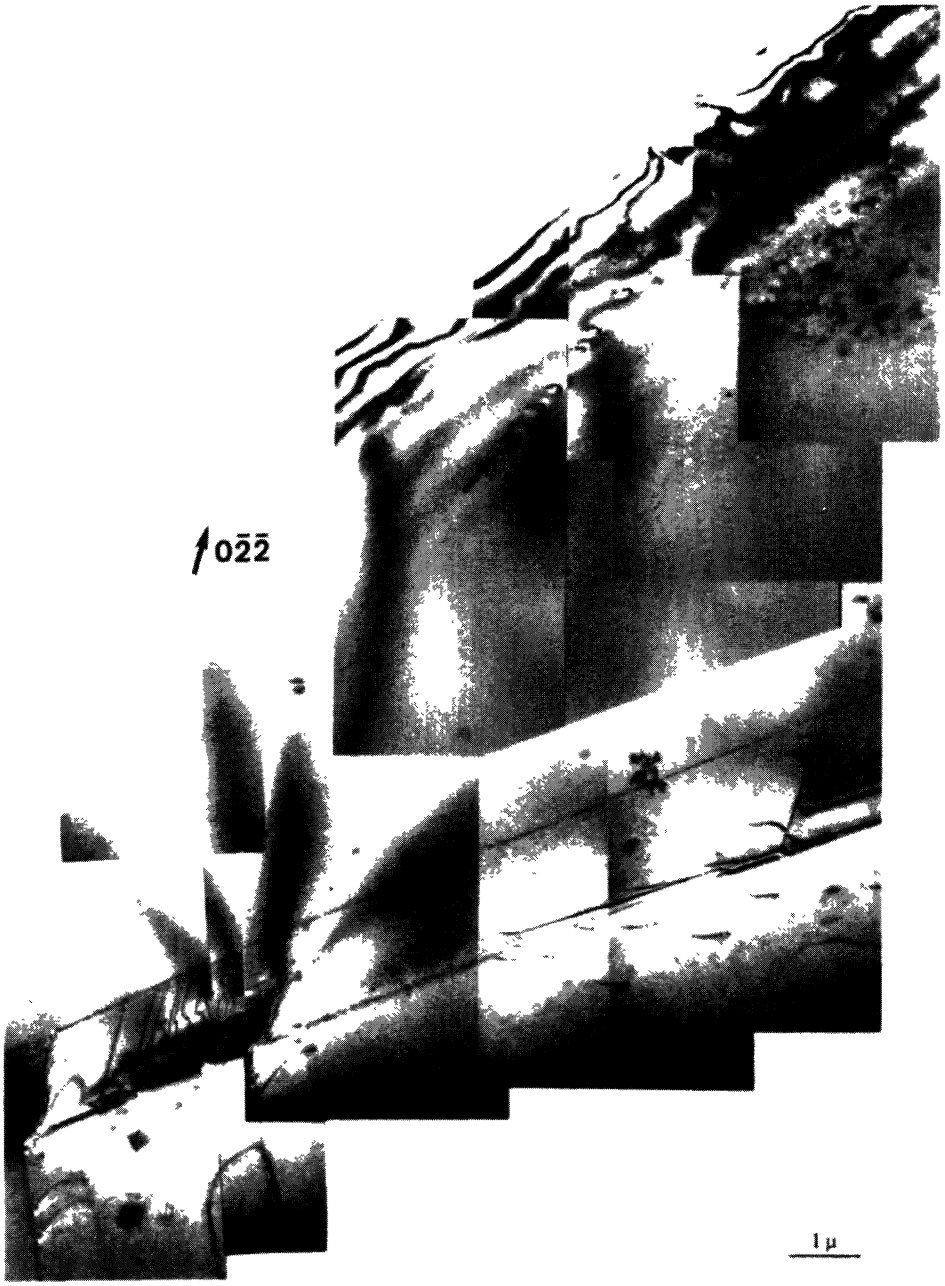

a

Fig. 8a.

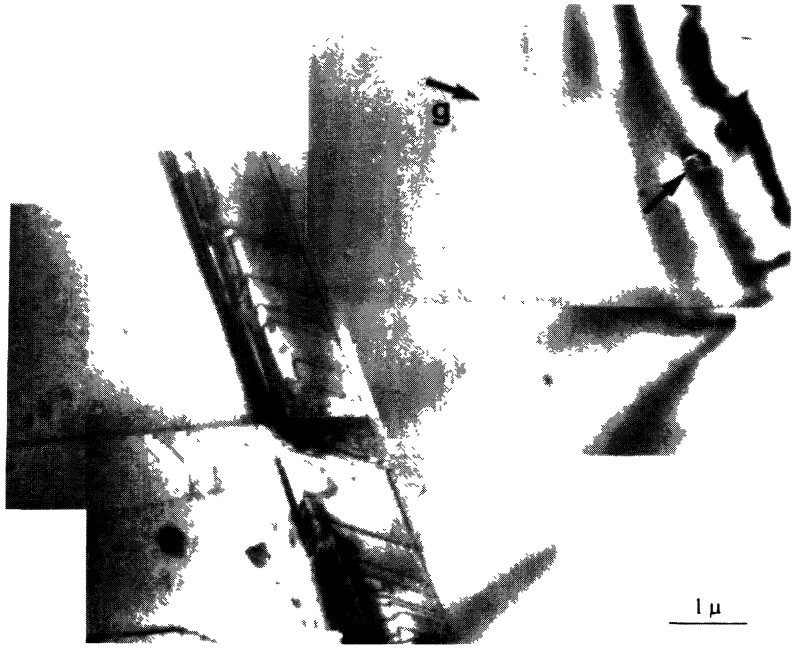

Fig. 8b.
Figure 8. — TEM observation of the configurations resulting from the interaction between $\Sigma = 51$ and the induced dislocations when the head partial is the 30° one. a) emitted dislocations (arrow) in the $(1\bar{1}1)_{II}$ plane and b) emitted dislocations (arrow) in the $(11\bar{1})_{II}$ plane. $g = [0\bar{2}\bar{2}]$.

The stress experiment was stopped after only a few dislocations were introduced into the GB. The sample was cooled down under load in order to freeze dislocation configurations.

3 mm disc HREM samples were then cut from the *in-situ* microsample. Then they were submitted to a slight ion milling thinning and finally to a chemical thinning (HF/HNO3-1/9 vol).

5.2 DECOMPOSITION OF A PERFECT DISLOCATION OF THE PRIMARY SLIP SYSTEM. — Decomposition of the in-coming dislocations was studied in details in [18]. In this paper we shall focus on the most frequently observed phenomenon: the decomposition of the perfect dislocations (with the 90° partial as the leading partial) of the primary slip system. (grain I as the reference).

Figure 11 shows clearly the two steps of the decomposition of a $a/2\,[\bar{1}10]$ bulk dislocation.

The first step is shown in figure 11a where the perfect dislocation is decomposed into two residual GBDs D_1 and D_2 following the scheme:

$$\begin{aligned} a/2\,[\bar{1}10] &= D_1 + D_2 \\ &= (3b_c + 2b_g + b_d) + 2b_g \\ 1.5h_0 &= 6.5\,h_0 + -5\,h_0 \end{aligned}$$

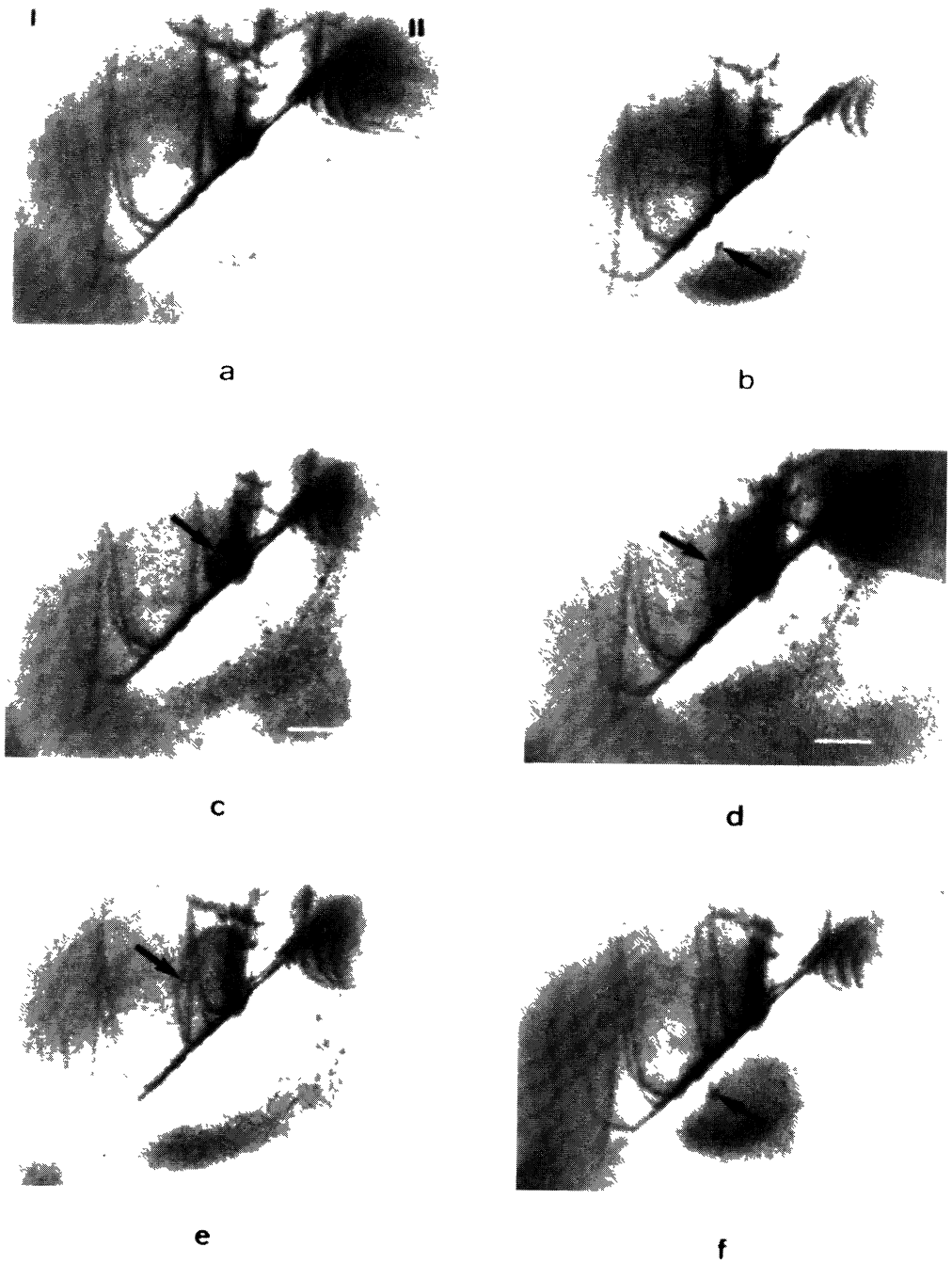

Fig. 9. — $\Sigma = 19$ *in-situ* deformation sequence in the conditions where the 90° partial is the head partial (θ increases). Marker = 1 μm.

a

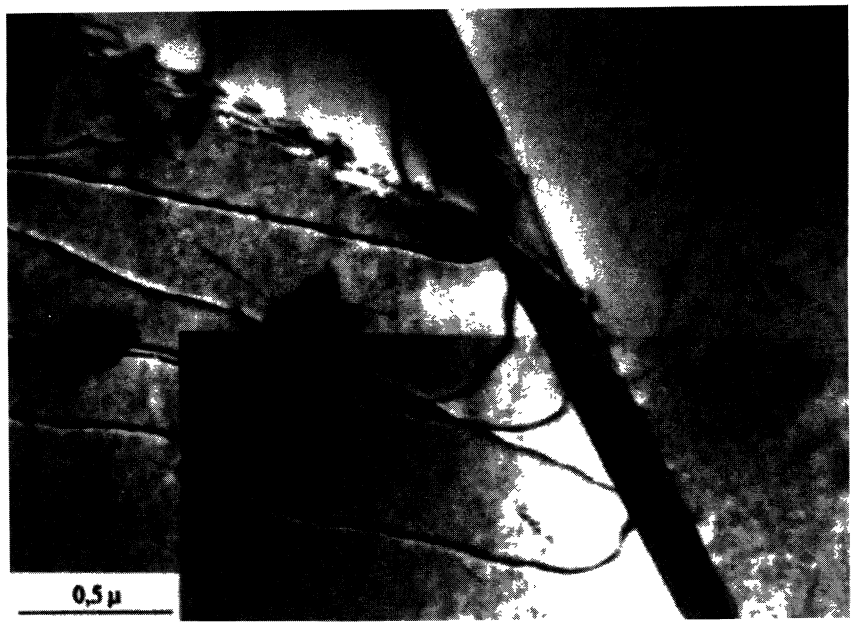

b

Fig. 10. — a) Weak beam observation $(g, 2g)$ of the emitted dislocations in $(11\bar{1})_{II}$ with $g = [004]_{II}$; b) TEM observation showing the perfect dislocation loop (arrow) emitted on the $(111)_I$. $g_I = [2\bar{2}0]$, $g_{II} = [2\bar{2}0]$.

with $h_0 = |b_c| = a/\sqrt{51}$. The b_c, b_g, b_d Burgers vectors corresponds to the $\Sigma = 51$ DSC vectors as shown on the figure 12. b_c, and b_g BVs are perpendicular to [011] whereas b_d as a component $a/4[011]$.

$$b_c = a/51\,[\bar{1}\,5\,\bar{5}]_I \quad b_g = a/102\,[\overline{10}\,\bar{1}1]_I\,, \quad b_d = a/102\,[\bar{5}\,25\,26]_I$$

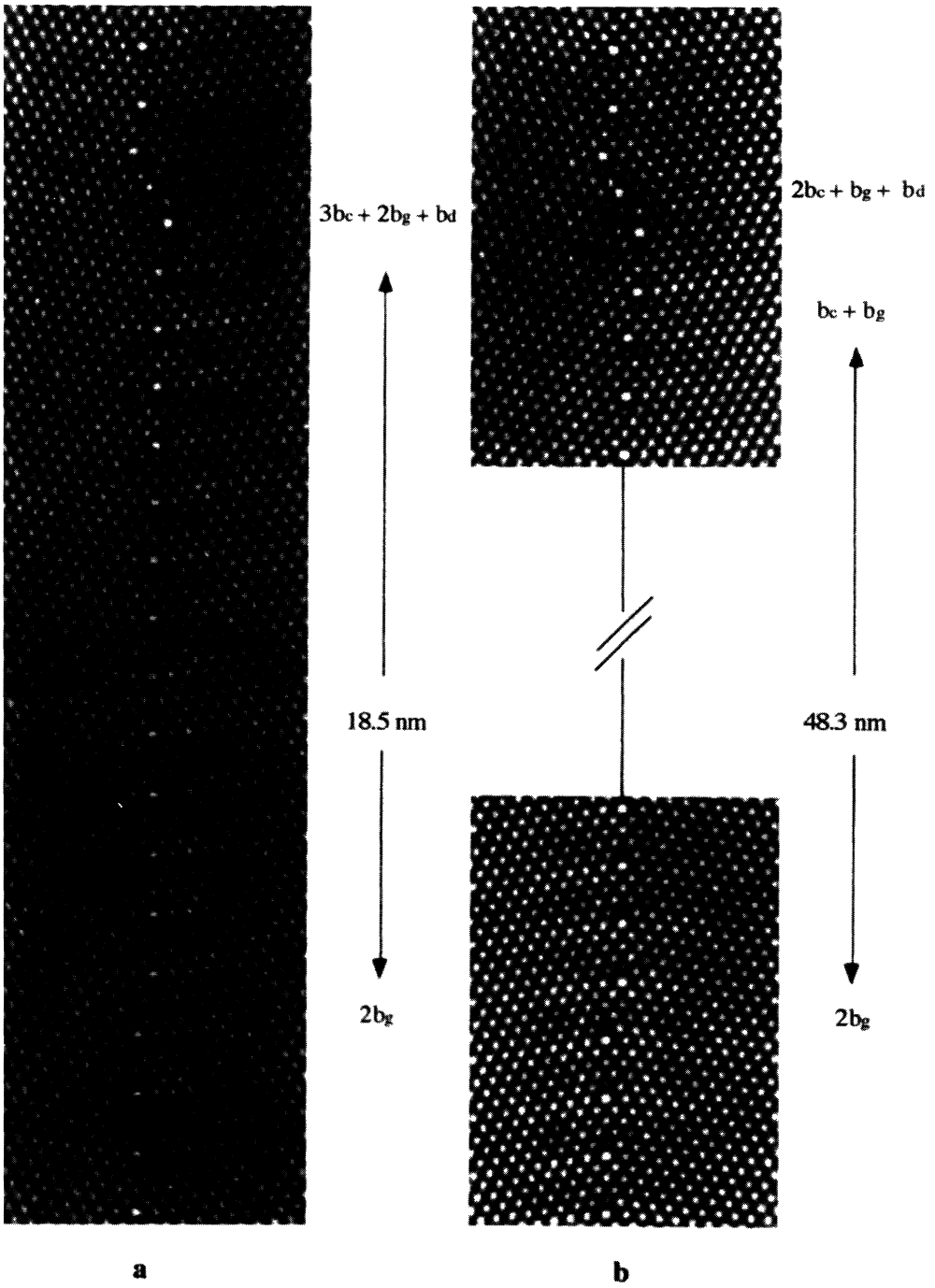

Fig. 11. — HREMicrographs of the two steps decomposition of the perfect dislocation coming on the primary slip plane. a) decomposition into two residues: D_1 and the glissile D_2. (2bg) b) decomposition by glide and climb of the D_1 residue; the D_2 glissile residue is far away from the impact point.

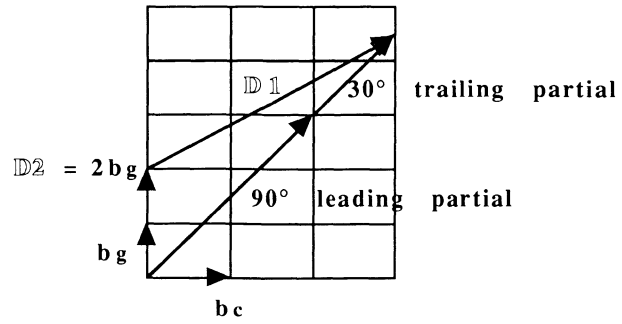

Fig. 12. — Partial view of the $\Sigma = 51$ DSC lattice projected along the [011] axis. The lattice is orthorombic with a centered face parallel to the GB plane with $b_c = a/51\left[\bar{1}5\bar{5}\right]_I$ and $b_g = a/102\left[\bar{1}0\ \bar{1}1\right]_I$. The first step of the decomposition of the in-coming dislocation (with the 90° partial as the head partial) is shown.

The $2b_g$ GBD is glissile along the GB plane. Such an emission of a glissile residue was previously observed by *in situ* [3] and HRE [4] microscopies in the case of the $\Sigma = 9$ deformation. Like in this case, the emission of the glissile residue occured as the 90° head partial touched the GB. However, unlike in $\Sigma = 9$, the elementary DSC glissile GBD is not observed. This may be due to the fact that the $\Sigma = 51$ b_g GBD is associated with a GB step whose height is 23 h_0 and consequently this would have led to a high GB step energy. On the other hand, the structure of the $2b_g$ is simple and closely similar to the $2b_g$ related to the $\Sigma = 19$ GB [17]. This can be understood by the similar symmetry of $\Sigma = 51$ and $\Sigma = 19$ (see Fig. 2 and Fig. 3 respectively).

In the second step (Fig. 11b) the D_1 residue is found to decompose by climb and glide into two GBDs (D_2 glissile residue has gliden away) following the scheme:

$$D_1 = (3b_c + 2b_g + b_d) = (2b_c + b_g + b_d) + (b_c + b_g)$$

$$\text{GB step} = 6.5\ h_0 = 4\ h_0 + 2.5\ h_0$$

Figure 11b shows the two intermediate residues separated by one half a period of $\Sigma = 51$. From a b^2 criterium, the gain in energy is very small. Thus the gain in energy by reducing the step height might be dominant. The core structure has also to be considered: as a matter of fact the $(b_c + b_g)$ residue is half a period of the $\Sigma = 33$ GB (which has a mirror glide symmetry and is intermediate between $\Sigma = 51$ and $\Sigma = 19$). This stable SU group (with a small GB step height) might reduce the energy.

6. Conclusion.

As compared to the $\Sigma = 9$ GB [1,2,4], the two $\Sigma = 51$ and $\Sigma = 19$ GBs might be considered as symmetrical "low angle" GBs with Lomer dislocations cores (L structural unit) separated by perfect crystal (C units). Thus their deformation behaviour might be thought to be different from the $\Sigma = 9$ GB one which reacts as a strong obstacle to slip transmission. From the *in-situ* electron microscopy, TEM and HREM observations, it was clearly established that, like in $\Sigma = 9$, the dislocations induced by the deformation interact strongly with the GB and that the transmission is not a direct process. The HREMicroscopy permits to clarify that point: like in the case of the $\Sigma = 9$ GB, the dislocations were stopped by the GBs where they decomposed. Although the number of possible residual GBDs is larger, the decomposition is governed by the structure as shown in

[19]. The transmission arises only at the head of a dislocations pile-up. As already discussed in [5] for $\Sigma = 9$ GB, it has been shown that the nature of the in-coming leading partial greatly influence the transmission process and the role of the GBD mobility being also to be accounted for. The resulting configurations have been compared via the elastic computations of their energy [18].

References

[1] BAILLIN X., PÉLISSIER J., BACMANN J.J., JACQUES A., GEORGE A., *Phil. Mag.* **A55** (1987) 143.
[2] JACQUES A., GEORGE A., BAILLIN J., BACMANN J.J., *Phil. Mag.* **A55** (1987) 165.
[3] BAILLIN X., PÉLISSIER J., JACQUES A., GEORGE A., *Phil. Mag.* **A61** (1990) 329.
[4] EL KAJBAJI M., THIBAULT J., *Phil. Mag.* **A58** (1988) 325.
[5] THIBAULT-DESSEAUX J., PUTAUX, BOURRET A., KIRCHNER H.O.K., *J. Phys.* **50** (1989) 2535.
[6] THIBAULT J., PUTAUX J.L., JACQUES, GEORGE A., ELKAJBAJI M., *Microsc.Microan., Microstr.* **1** (1990) 395.
[7] SUTTON A., VITEK V., *Phil. Trans. Roy. Soc. London*, **A309** (1983) 1, 37, 55.
[8] COUJOU A., LOURS P., CAILLARD D., CLÉMENT N., *Acta Met.* **38** (1990) 825.
[9] PÉLISSIER J., LOPEZ J.J., DEBRENNE P., *Electron Microsc.* **4** (1980) 30.
[10] STADELMANN P., *Ultramicroscopy* **21** (1987) 131.
[11] LANCON F., Thèse d'Etat, Grenoble (1989).
[12] ROUVIÈRE J.L., Thèse de l'Université de Grenoble (1989).
[13] KEATING P., *Phys. Rev.* **149** (1966) 674.
[14] BARAFF G., KANE E., SCHLÜTER M., *Phys. Rev.* **B21** (1980) 5662.
[15] BACMANN J.J., GAY M.O., de TOURNEMINE R., *Scripta Met.* **16** (1982) 353.
[16] PUTAUX J.L., Thèse, Université de Grenoble-France (1991).
[17] THIBAULT J., PUTAUX J.L., MICHAUD H.M., BAILLIN X., JACQUES A., GEORGE A., *Inst. Phys. Conf.* **117** (1991) 105.
[18] MICHAUD H.M., Thèse de l'Institut National Polytechnique de Grenoble (1991).
[19] THIBAULT J., PUTAUX J.L, JACQUES A., GEORGE A., MICHAUD H.M., BAILLIN, (1993), *Mater. Sci. Eng. A* (under press).